Plasma Chemistry and Plasma Processing, Vol. 26, No. 1, February 2006 (© 2006)
DOI: 10.1007/s11090-005-8727-2

A Critical Assessment of Particle Temperature Distributions During Plasma Spraying: Experimental Results for YSZ

T. Streibl,[1] A. Vaidya,[1] M. Friis,[1] V. Srinivasan,[1] and S. Sampath[1,2]

Received February 17, 2005; revised August 22, 2005

Plasma sprayed coatings of ***Y****ttria* ***S****tabilized* ***Z****irconia (YSZ) have been studied extensively through the years to understand variations in coating properties as well as to achieve control on microstructure of the coatings. The requirement for microstructural control and reliability have become all the more important as coatings have now become part of an integrated "prime reliant" design strategy aimed at increasing turbine inlet temperature and associated efficiencies. One of the important thrusts in monitoring and controlling the process has been the application of process sensors that measure spray stream characteristics, notably particle temperature and velocity. Although single particle-based measurements have been available for some time, in general control strategies based on particle state rely on average values of temperature and velocity. In this study, a detailed examination of particle temperature distributions is presented. When systematically examined over a wide range of operating conditions of the resulting range of particle temperatures, a significant structure in the statistical distribution has been observed. A close inspection of the data indicates that this distribution can be interpreted as melting state indicator for YSZ. A characteristic peak at the melting point of* ZrO_2 *(error in absolute* T*-measurement is* $\approx \pm 10\%$*) can be used as an indicator for re-solidified particles. In the past, control strategies based on process diagnostic sensors have been based on average particle temperatures and velocities. Although the average values seem to be promising as control parameters, it has been shown through our results that different melting states could be demonstrated for the same average* T *and* V *settings. The melting state in turn has an important bearing on the coating structure and properties. It therefore implies that a process control strategy (to maintain coating quality) based on in flight particle sensors will have to take these findings into account. As an example, one strategy of process control would not only define the process in terms of the average particle temperature and velocity but also include the effect that parameter changes have on distributions.*

KEY WORDS: Plasma spraying; particle temperature; experimental.

---

[1] Department of Materials Science and Engineering, Stony Brook University, Stony Brook, NY 11794, USA.
[2] To whom correspondence should be addressed. E-mail: Sanjay.sampath@sunysb.edu

1. INTRODUCTION

In recent years, a number of robust, user friendly particle diagnostic tools have become available for thermal spray processes. These have significantly enhanced our ability to monitor the processes. These particle diagnostics tools allow assessment of inflight particle temperature, velocity, and trajectory and to a limited extent, particle diameter distribution (particle diameters are indirectly inferred from thermal emission and the principle does not take into account shape or phase change). Broadly, two techniques of measurement are followed: the one based on individual particle measurements and another set based on ensemble measurement methods. Typically these sensors work on the general principle of two color optical pyrometry and time triggered measurements of velocity. Detailed discussion of these sensors is available in literature – e.g. DPV 2000,(1,2) LDA,(3) PSI(4,5) for the single particle based techniques and SPT & IPP,(6–8) Spray Watch,(9) Accuraspray,(10) ensemble apparatus similar to DPV,(11) PFI(12) for ensemble based techniques.

As these technologies have matured and become cost-effective, there has been a significant increase in their utilization. The principal reason for this is the increasing need to enhance process reliability, reproducibility and to ultimately meet the goal of producing prime reliant coatings. Although thermal barrier coatings have been the most significant candidates for these developments, numerous other opportunities exist on the horizon that can benefit from these improvements. To meet these future goals there are two principal requirements:

- Producing reliable and reproducible particle state(s). For a fixed torch geometry, the particle parameters are controlled by torch operating conditions, particle injection and plume location. Other events such as electrode (in particular, the anode) wear and resulting instabilities in the plasma jet can introduce random fluctuations that can be detected through particle state assessment. The nature of plasma spray processing introduces time-dependent phenomena at many different time scales. For example, the arc root fluctuations and time of flight of particles are in the milliseconds range, torch pass rates and build up of the deposit are of the order of seconds and degradation in the torch hardware is typically over many hours. Together with the stability of operational parameters, these time-dependent factors have to be considered to achieve the required particle state.
- The second requirement is to achieve reproducible deposit characteristics. This not only requires a 'reproducible' particle state but

> also the linkage with coating build-up process. i.e. considerable variability exists in the stochastic splat-based build-up process which is not only controlled by particle states but also through substrate condition, environment and movement of torch with respect to the substrate.

There is considerable activity around the world to address the above two attributes both from scientific as well as engineering points of view. A variety of efforts over the last few decades have addressed the particle state(13) and its implication on coating build up – both numerically and experimentally.(14) Several reports on successful correlation between particle properties and coating microstructure have been made.(15–22)

At the Center for Thermal Spray Research (CTSR) at Stony Brook, a concerted, integrated effort is underway to systematically link the phenomena and variabilities for the various sub-processes. The ultimate goal is to develop 'process maps' which will provide a scientific framework to assess effects and variabilities. These process maps have been divided into two distinct regimes. The 'first order' process maps link particle states to process conditions, while 'second order' process maps aim to link particle states with deposit state (in conjunction with some attributes of the substrate condition).(23–27)

1.1. The Particle State

While the various particle diagnostic techniques are clearly important for better process control, reproducibility and understanding, a deeper insight into diagnostics and the correct interpretation of sensor and diagnostic data is required.

It is widely appreciated that particle temperature and velocity are important parameters in determining the nature of coating build-up process. Particle temperature values with respect to the melting point of the material under consideration determine deposit build-up, efficiency and splat morphology. Particle velocity and temperature also determine the extent of spreading (flattening) and the nature of splat–substrate and splat–splat contact. Considerable work on these aspects points to the fact that the final microstructure is dependent on the particle melting state and kinetic energy. Many researchers have provided experimental evidence and models describing the complex phenomena of splat flattening, spreading and fragmentation.(22,28–30) These experiments and models correlate the splat characteristics to particle state through non-dimensional parameters such as the Reynolds, Jakob, Weber and Biot numbers.(31–33) While the models allow for a fairly detailed description of the particle state in-flight and also upon impact, the application of these models to experimental measurements is difficult.

In fact, a direct measurement of the particle melting state is nearly impossible since pyrometric techniques only provide access to the surface temperature. For instance, for low thermal conductivity ceramics such as YSZ, the surface can begin to evaporate even before the core melts. Such large gradients are generally unique to low conductivity materials such as refractory oxides where the particle surface temperature is not adequate to describe the melting state. Clearly a more complete estimate of the particle status is needed.

Vaidya *et al.* initially proposed a group parameter termed Melting Index to capture the melting state.(34) Zhang *et al.* followed with an analytical determination of melting index formulation rendering it non-dimensional.(13) Reynolds number provides a reasonable assessment of the kinetic energy parameter. Vaidya *et al.* further proposed a MI-Re-based 1st order process map and this in turn was a more accurate descriptor of the particle states. These studies have been made possible through the availability of single particle based sensor systems such as the DPV 2000. Another interesting approach is to perform measurement of indirect melting indicators like changes in particle shape.(4)

In addition to the fact that the temperature and velocity of particles may be inadequate to fully correlate to the splat and coating structures, it is equally important to understand the limitations of utilizing their average values for controlling and monitoring the process. As will be discussed in this article, when average values of the particle conditions are the only attributes measured or controlled, the resulting spray stream can be very different with respect to other crucial parameters that describe the property distributions.

A series of systematic studies to obtain ‘first order’ process maps for various YSZ powder morphologies were carried out. In an effort to allow cross-comparison of morphologies, the powder injection was ‘optimized’, to achieve the maximum permissible temperature and velocity at a given torch condition. This procedure ensured that the diagnostic instruments measured the influence of plasma gas on the particles, rather than the influence of different particle trajectories. In addition, this procedure permitted the elimination of carrier gas as a control factor from the experimental design.

In a series of experiments involving variations in both powder morphologies and process conditions, certain peculiarities in particle temperature distributions were observed. Similar results have been observed in the past but a detailed assessment of these distributions has not been undertaken. Friis *et al.*(35) reported variations in the width of particle property distributions (standard deviation) that were accounted for by changes in the spray gun parameters. Further observations and reports concerning distributions of the particle properties can be found in the literature,(36,37) but usually the number of acquired particles was insufficient to display detailed underlying patterns in the distributions. The particle temperature distributions at the effective spray distance (130 mm in this case) showed a multi-modal distribution. The number density across the different modes changed with process conditions. These findings suggest that there is a melting state indicator in the distribution that will allow new approaches to process control. In the current paper, a beginning towards this is attempted by explaining the changes in features found in particle temperature distributions as melting state indicator. It will be shown that the presence of a significant peak (named as 'G1' for reference) near the melting point of ZrO_2 can be used for this purpose. This aspect has been comprehensively discussed in the current article. Additional insight into particle classification with respect to temperature and size is also provided. Essentially, the overall spread of feedstock within different temperature zones is revealed through this analysis.

This article focuses on a narrow set of experiments that were geared towards building an overall understanding of the process. As such, it is important to realize that reliable data for this experiment and analysis have depended on the cornerstones of the following procedures:

- Sufficiently large data set (that allowed resolution of the overall distribution into component ones) comprising of single particle properties (acquired with the DPV 2000 instrument).(38)
- A 3D multiple sensor set up with careful instrumental and spatial calibration to allow for redundancy and complementary data acquisition.
- Detailed analysis that involved capturing plume characteristics in the cross section of the particle spray stream (scan and point measurement combined).
- Ensuring optimized injection for each spray condition across different powder morphologies.

While each of these topics would be of considerable interest, the focus of this present set of papers is to critically examine the in-flight particle temperature. The first paper presents the experimental findings and analyses the various scenarios that could yield the observed distributions. Particle size, morphology, spray parameters were all varied as part of this exercise. A complementary article (titled "A Critical Assessment of Particle Temperature Distributions During Plasma Spraying: Numerical Studies for

YSZ") presents the 3D numerical modeling that was used to track the particle temperature distributions and confirms the experimental findings and the proposed physical phenomenon.

2. EXPERIMENTAL PROCEDURE

2.1. Processing

The Feedstock material used was 8 wt% Y_2O_3-stabilized ZrO_2 with three different powder morphologies, namely, dense spherical, hollow spherical and dense angular. These materials were chosen because of their wide usage and interest in the thermal spray industry. As a continuation of this study, a detailed analysis of the microstructures generated from these feed stocks is also being examined.

All experiments were performed using a Sulzer Metco 7 MB plasma torch equipped with a 'G' nozzle that has a diameter of 8 mm (Nitrogen was used as primary and carrier gas and hydrogen as the secondary gas). Powder injection was through a 1.8 mm diameter injector located 2 mm from the face of the nozzle. The injection was orthogonal to nozzle axis and in the downward direction.

2.1.1. Part I:

The gun parameters – current, primary and secondary gas were varied between their respective minimum and maximum levels (Table I). The full parameter range and variation of the gun was explored in a total of 30 parameter settings (where the combination of parameters was laid out according to a modified central composite design strategy). In this manner, the complete attainable range of particle temperature and velocity was explored.

2.1.2. Part II:

Results from previous studies were used to build empirical correlations between the control process parameters and particle response parameters, namely the average velocity and temperature.

Table I. Plasma Gun Parameter Extremes

Parameter	Minimum	Maximum
Current (A)	466	634
Nitrogen (Slpm)	32	64
Hydrogen (Slpm)	1.7	12

From these relations, it is seen that identical mean particle properties can be achieved by *widely different* control parameter settings. Five such settings were used to attain identical mean particle temperature and velocity. For each of these five settings, detailed diagnostic measurements were made. Coatings were also fabricated for these conditions for further microstructural and property measurements.

2.2. Diagnostics

Detailed diagnostic characterization of the spray plume was carried out using multiple sensors. The sensors used are ‘SPT’ (a line camera to measure the location of the plume), ‘IPP’ (ensemble measurement of the plume temperature) and the “DPV 2000” (for single particle measurements). This approach provides redundancy, complementary data acquisition and the opportunity to cross correlate data from different instruments. A schematic of the layout is provided in Fig. 1.

Although the current article presents detailed analysis of data obtained from the DPV 2000 system, for the sake of completeness, the experimental procedure is described with all the sensors used. Data from the SPT and IPP sensors is not presented here in any detail but it is important

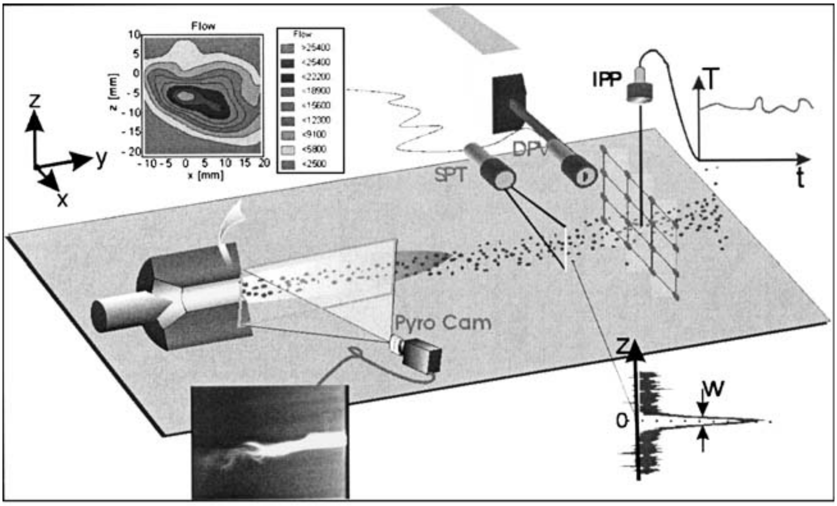

Fig. 1. Schematic of the layout of the diagnostic sensors used for characterizing the plume. The different sensors used are depicted at their point of measurement (with respect to the plasma torch axis) along with their typical data output.

to mention that the quick feed back from these sensors was utilized to achieve proper injection of the feed stock.

The DPV 2000 sensor head used in this experiment is configured to measure over an area of 0.14 mm^2 with a depth of field of 1.9 mm. A large number of particle measurements were acquired (>10,000) with the DPV 2000 at a given location. This allowed an optimization of the histogram bin size to provide an efficient and unbiased estimate of the particle temperature probability function.(38) Bin size of 10°C was chosen in order to resolve structures in the particle temperature distributions.

3. RESULTS AND DISCUSSIONS

3.1. Analysis of Temperature Distributions

3.1.1. Salient Features of The Distributions

Typical histograms of size, velocity and temperature of particles acquired in the plume flow center at spray distance are shown in Fig. 2. The distributions in this figure resulted from a feed stock that had the original size distribution as shown in Fig. 3. It can be seen that the particle size and velocity distributions behave as expected, i.e. the particle size resemble the original feedstock distribution and the velocity distribution constitutes a typical Gaussian distribution centered on the mean velocity. Concerning the particle temperature, the individual particle temperatures vary over a large range ($\approx$ 800°C) as expected. This is due to the distribution in particle size and associated thermal and kinetic history (i.e, trajectory, dwell time). Of particular note is the fact that the distribution displays multiple peaks. The overall particle temperature distribution can be readily explained by three overlapping Gaussian distributions with corresponding peaks, here denoted as 'G1', 'G2' and 'G3' (ordered in sequence of increasing temperature). We present below an analysis of these sub-distributions and examine their physical origins. In the following sections we systematically consider various effects that could have resulted in the multimodality of particle temperature distribution and present an analysis for each of these cases.

3.1.2. Variations in Particle Distributions Through the Complete Process Space

Figure 4a depicts 15 experimental points represented by their respective average temperature and velocity. This data set was obtained when the experiment was carried out as described in 'Experimental Procedure, Part I'. The vectors demonstrate how particle velocity and temperature are

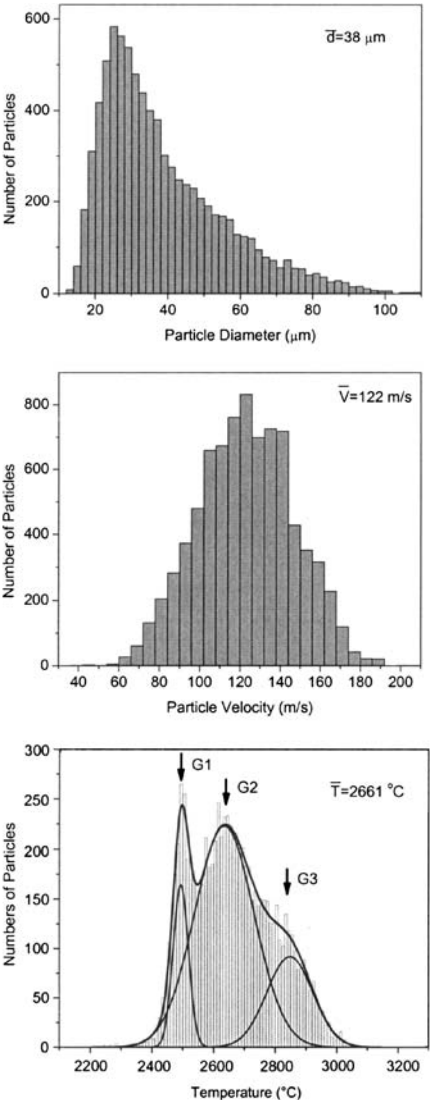

Fig. 2. Typical distributions observed for different particle attributes of size, velocity and temperature. Average values of the distributions are also listed. The overall temperature distribution curve has been represented as a sum of three Gaussian curves and the individual peaks of these underlying curves have been labeled as 'G1', 'G2' and 'G3'. (The feedstock for this experiment was an 'angular dense' powder and the spray parameters were: 47.6 SLM of N_2, 5.6 SLM of H_2, 550 A current and 3.7 SLM of carrier gas).

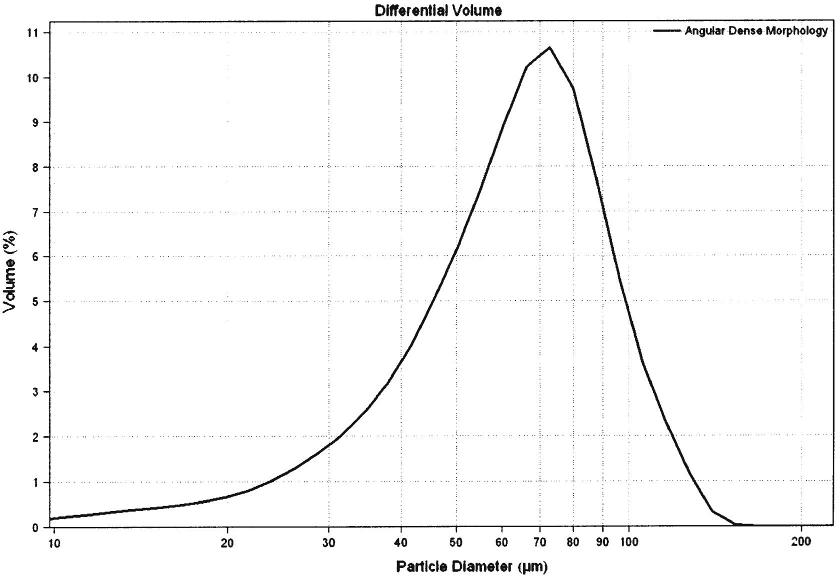

Fig. 3. Particle size distribution of the original feed stock (size, velocity and temperature distributions of this material for one spray condition have been provided in Fig. 2).

influenced by an increase (moving from – to +) or a decrease (moving from + to –) in the parameters – current, primary or secondary flow rate. In this figure, the points have been labeled in alphabetical sequence following an increasing average temperature order. These experimental points thus form a subset of the complete larger systematic study of the correlations between gun parameters and particle properties, i.e. a 'first order' map, (specifically for the 'angular dense' morphology). Figure 4b examines the change in particle temperature distribution for these 15 points (arranged from the lowest to highest average temperature). Histograms were created with a bin size of 10°C, but for clarity we only display a fitted curve of the particle temperature distribution.

For the case presented in Fig. 4, the following comments should be noted regarding the accuracy of measurement. In order to examine repeatability, eight measurements at fixed operating parameters were randomly distributed throughout the experiment (which was carried out over a 3.5 h period). The values were clustered around the point 'I' in Fig. 4a with a range of ±13°C and ±2.5 m/s. These numbers are representative of the stability of the process itself (including aspects such as gas flow and power fluctuations and hardware degradation) and have no relation to the

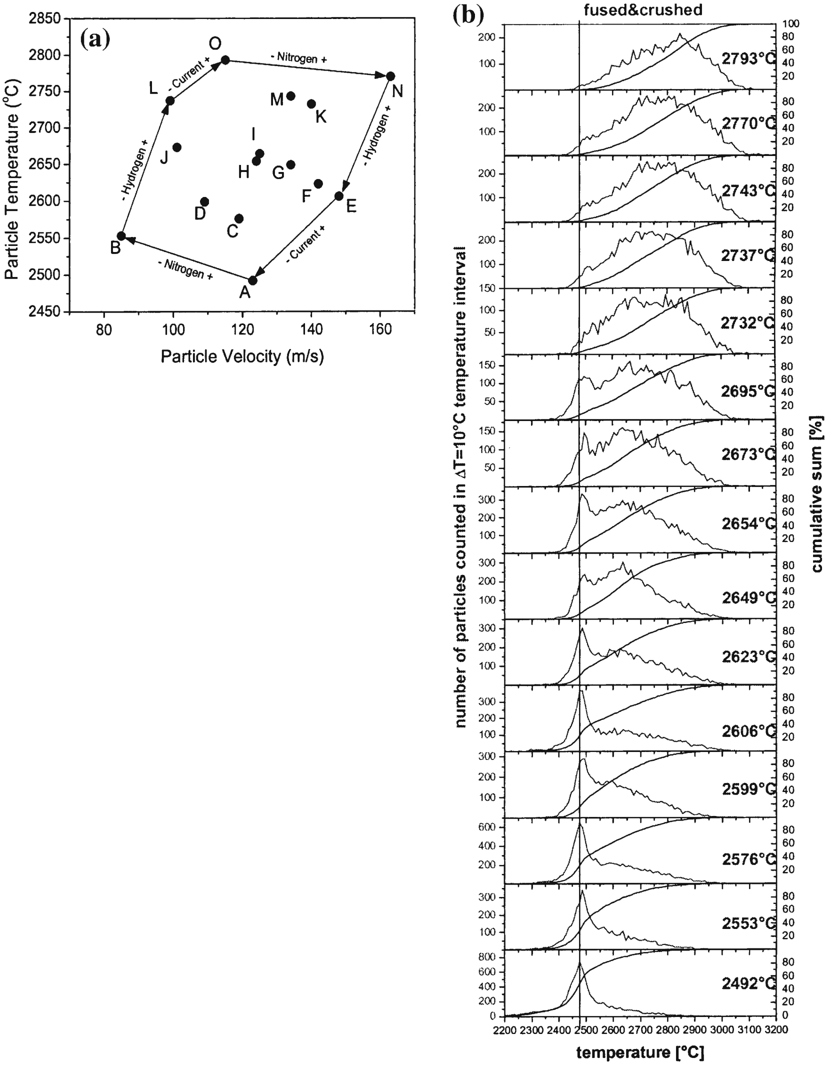

Fig. 4. (a) Maximum obtainable particle temperature and velocity range for the plasma torch and operating conditions as described in the text. (b) Individual particle temperature distributions sorted by increasing average particle temperature (low at bottom, increasing from A through O.). This data is for the 'angular dense' morphology.

accuracy of measurement of the instrument. The error in measurement of the instrument is a cumulative value comprising of

- Variation in emissivity as a function of the wavelength.
- Statistical response of the detector.
- Spatial variation in particle location (which results in a change in spectral radiant power delivered to the detector).
- Calibration error of the pyrometer.

These aspects have been addressed in detail by Fincke *et al.*(6) and Ng.(39) The DPV 2000 reference manual provides information regarding the accuracy of measurement of temperature as a function of the emissivity and particle diameter. From the charts provided in the manual, and comparing the temperatures attained in our experiments, the accuracy of measurement would be better than ±7%.

There is a question regarding the effective zone of measurement (from within the zirconia particles) that contributes to the radiation detected by the pyrometer. Considering the three conditions of particles that can exist in the spray stream – solid, partially molten and fully molten – the radiated intensity as detected by the pyrometer is dependent on the optical properties of solid and liquid zirconia. In previously published research paper, Ng *et al.*(40) have analyzed and presented results of the case of multi-wavelength pyrometry applied to optically transparent materials. They have demonstrated that when the principle is implemented by acquiring the spectrum over a large range of wavelengths, it is possible to distinguish the contribution from the surface and from the bulk of a transparent material. With the limitation of data acquired over only two wavelengths (as in our case), this analysis cannot be carried out. The problem is also compounded by the fact that the optical properties such as absorptivity, reflectivity and the refractive index are dependent on the chemistry of emitting zone, wavelength being considered and also the temperature of particle. Some guidelines to the role of these factors have been provided by Petrov(41) and Dombrovsky.(42) It has been shown that there can be as much as 200–300 K difference in temperature between the measured and actual value due to non isothermal heating of semitransparent particles. All of our following observations and hypotheses are based on the understanding that the overall data may be biased in absolute values due to the factors mentioned here in. However, a relative comparison across different plasma conditions and over the temperature region of interest can still be made to observe the pattern changes. Furthermore, the physical phenomena leading to these differences may also be conjectured from this examination (as provided below).

The characteristic features of temperature distribution seem to be quite independent of the different particle velocities (although velocities and therefore, in the first approximation particle dwell time change by a factor of two over this range of particle conditions). Figure 4b shows that at low average particle temperatures, the distributions are dominated by the significant peak 'G1' at a constant temperature of 2475°C. This Gaussian sub-distribution loses intensity with increasing average temperature, resulting in more particles shifting toward the high temperature Gaussian distributions 'G2' and 'G3'. Above an average particle temperature of approximately 2730°C (distribution 'K') the 'G1' structure disappears completely and all particles can be found in the structures 'G2' and 'G3'.

From the sequence of distributions, it seems likely that the first peak, 'G1', originates from the melting temperature. Considering that ZrO_2 is a refractory material with poor thermal conductivity and large latent heat of fusion, it can be expected that a large fraction of particles are stalled at one specific temperature. The existence of a peak in the temperature distribution located at the liquid–solid phase transformation can be understood from a statistical point of view. Ideally during an equilibrium phase transformation, the temperature of a material stays constant at the melting point until the latent heat of fusion is either added (melting) or removed (solidification) from the material. Thus, the probability of detecting particles at the melting point would be higher (compared to any other temperature value). As a consequence of this phenomenon, the diagnostic measurement instruments pick up a larger number of those particles that are resident at the melting point. The presence of this peak seems to be a confirmation that heat transfer to the particle (at the spray distance of 130 mm) is close to equilibrium and that the thermal gradient within the particles is negligible.

3.1.3. Comparison Across Different Feed Stocks

It has been seen that the particle condition in terms of the temperature and velocity varies considerably when different feed stock morphologies of YSZ are injected into the plasma flame (at exactly same operating conditions). In order to examine the general nature of this phenomenon, similar experiments were performed for two other powders with similar size distributions but different morphologies (as described in the experimental section).

Figure 5 shows the corresponding response of these powders with respect to the overall range as well as a comparison of select temperature distributions. Examining the top part of this figure, it is evident

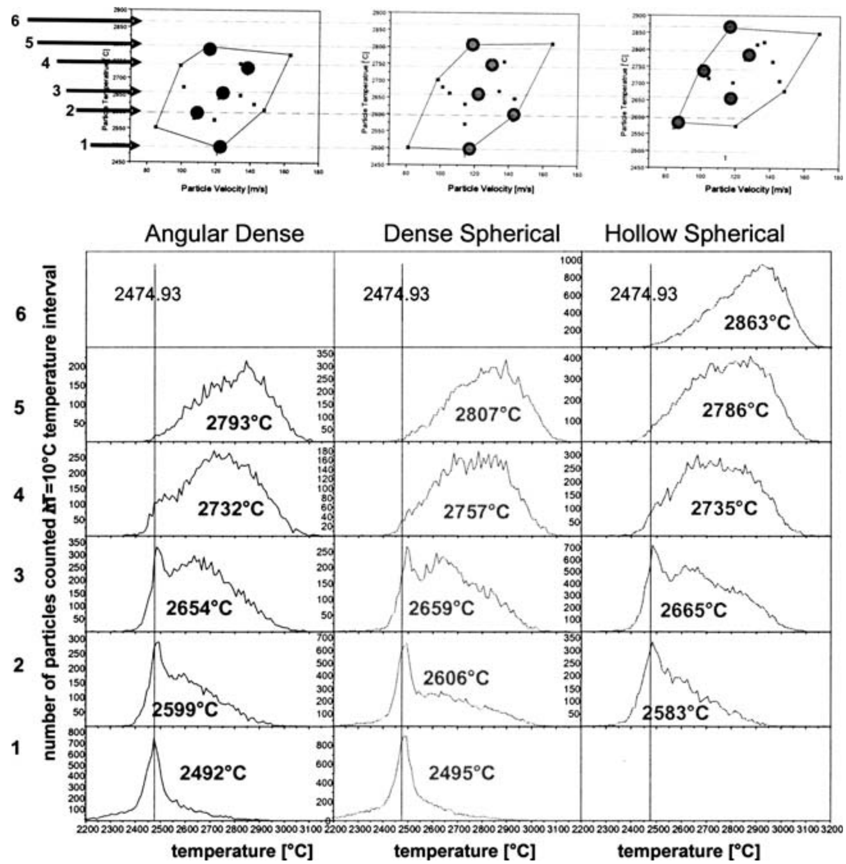

Fig. 5. Comparison of temperature distributions for angular, dense spherical and hollow spherical morphologies. The top charts depict the overall range of particle temperatures and velocities attained by each morphology. Distributions within the same row (labeled 1 through 6) have similar mean temperatures.

that the different powders exhibited quite similar particle temperature and velocity ranges with the exception of the hollow spherical particles, which had approximately 100 degrees higher average temperature than the two other morphologies. This is due to the lower mass and the hollow sphere construction of the particle, which insulate the shell from the core by a gas layer. The small mass of the hollow particle surface therefore heats up rapidly, melts and superheats.

Five experimental points with similar average temperatures were chosen for each powder and their corresponding temperature histograms are shown in Fig. 5. The characteristic peak 'G1' occurs in all cases at the same temperature (2475°C). In addition, the different powder morphology temperature histograms display identical shapes for similar average temperatures. As can be seen in Fig. 5, with increasing temperature, the intensity of 'G1' peak is lowered and again it vanishes at the same temperature level for all feed stock morphologies.

It is noteworthy that similar average temperatures display similar distributions for vastly different powder morphologies, indicating that once the particles are heated up, the sensors cannot separate or recognize different powders, rather they appear to be the same once melting begins. The peak 'G1' appears at identical temperatures and the distributions are similar for similar average temperatures for the different powders. This further indicates that melting point of the material must be the origin of peak 'G1' since material of the powder is same.

3.1.4. Examining Particle Size Effects

3.1.4.1. Dependence on Trajectory. All experiments corresponding to the histograms A–O, used the same batch of powder and hence the size distribution of the feed stock was same. Moreover, the powder was injected using a methodology to set the carrier gas so that particles travel along a similar trajectory for all plasma conditions. The average temperature differences measured are therefore due to changes in the plasma conditions and not due to different trajectories or different particle size. For the experimental points A–O, the average particle size measured was very similar ranging randomly from 34–40 μm, and the overall size distributions did not show significant variation (size range for all morphologies was the same). It is important to note that this range is comparable to the error of size measurement with the DPV, reproducibility of size between different runs at the same operating condition and dependence of average size from injection. As such this range is too small to make a conclusion about the vaporization of particles. There is also the bias due to a preference of detection towards the large and hot particles (the small and cold particles are not recorded). Keeping all this in mind, we can assert that even if there is some size classification of the feed stock that occurs in the spray stream cross section, it is not the cause of the difference in temperature distributions.

3.1.4.2. Dependence on Size Selection. It could be argued that a significant peak structure may occur at a particular temperature if there is some bias in size selection such that a large number of particles of one

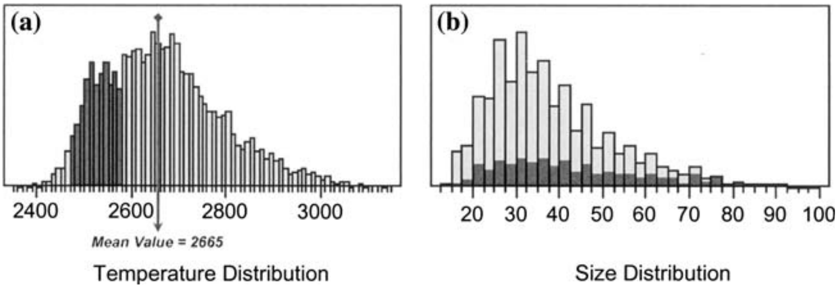

Fig. 6. Temperature and size distributions with all particles comprising the first peak in temperature histogram selected. The corresponding particles are highlighted in the size distribution chart also.

size are detected. In Fig. 6a, a sample temperature distribution has been depicted such that the particles that have temperature close to the peak 'G1' are highlighted. The corresponding size of these particles is highlighted in Fig. 6b. As can be seen, the first peak 'G1' comprises of particles of all sizes and is not an artifact of any single sized (or a narrow size range) particles. These two charts taken together clearly indicate that the presence of first peak is not governed by a bias in the particle size. A similar analysis of the other peaks revealed that particles at or near each of those peaks were also distributed throughout the size range. From this it can be concluded that the peaks G1–G3 are not a particle size artifact.

It is important to note that although size affects the particle temperature (in the sense that small particles tend to have higher temperatures and large particles tend to have low temperatures), this tendency is rather small (with a correlation coefficient of about 0.25). By itself, this segregation effect does not provide a complete explanation of the structure of the temperature distribution. Taken together with the physical phenomenon of melting or re-solidification, it confirms that the larger particles are harder to fully melt/resolidify, and remain at the melting temperature for a prolonged period of time.

Additional insight can be gained through calculation of the melting index (M.I.) distributions.(13) The original idea of creating a melting index was to normalize the particle temperature with respect to particle size and particle dwell time in the plume. The calculation of M.I. is described by the equation below

$$\text{M.I.} = \frac{\Delta t_{\text{fly}}}{\Delta t_{\text{melt}}} = \frac{24k}{\rho h_{\text{fg}}} \cdot \frac{1}{1 + 4/Bi} \cdot \frac{(T_{\text{f}} - T_{\text{m}}) \cdot \Delta t_{\text{fly}}}{D^2}$$

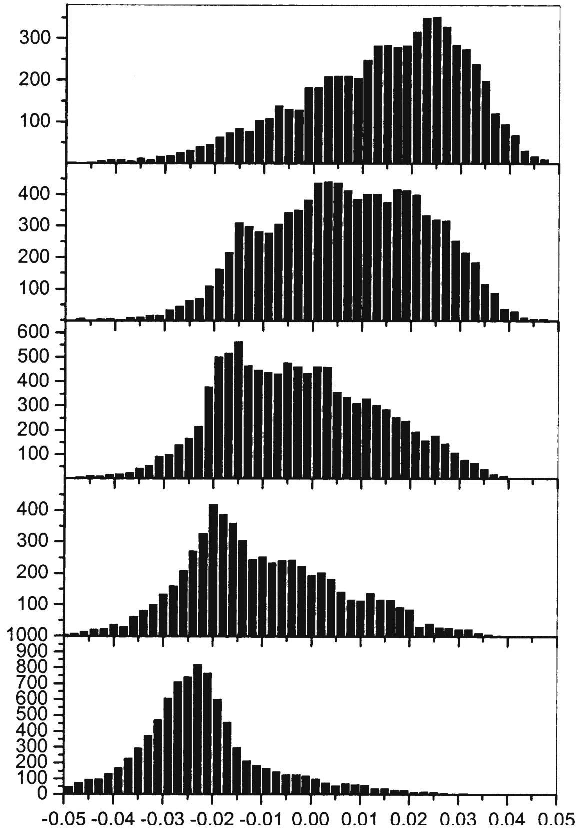

Fig. 7. Melting Index distributions for the angular dense feed stock material corresponding to the temperature distributions shown in Fig. 4.

where, k is the thermal conductivity of material, ρ is the density, h_{fg} is the enthalpy of fusion, Bi is the Biot number of the particle, T_{f} is the measured temperature of the particle, T_{m} is the melting point of the material, D is the diameter of the particle and Δt_{fly}, is the estimated time of flight of the particle from injection point to the measurement point.

The M.I. distributions are as shown in Fig. 7. It can be seen that the basic structure of the temperature distributions is retained in this sequence of charts also. The threefold structure from temperature distributions still exists thereby implying that real melting state transitions are being tracked.

3.1.5. Examining Effect of Different Plasma Torch and Plasma Gases

3.1.5.1. Argon – Hydrogen Conditions. In order to eliminate the possibility of these peak structures originating from experimental set-up of the plasma generator, the plasma chemistry or the particle diagnostic instrument, a prior experiment was re-examined in light of the new findings.(43) In this experiment, the plasma torch was operated with an Ar–H_2 plasma for a different feed stock material of ZrO_2, where the data was acquired at a stand-off distance of 70 mm, using a different model of DPV 2000. Five conditions were selected and the temperature distributions are presented in Fig. 8. The distributions are once again sorted with respect to increasing particle mean temperature (from bottom to top). Although the number of acquired particles was relatively low (600–1600), the distributions clearly exhibit similar structures as in the N_2–H_2 plasma. As described earlier, the temperature controlled distribution change from the dominant peak 'G1' to the structures 'G2' and 'G3' is obvious.

It can be seen that the peak 'G1' occurs at a different temperature in the argon–hydrogen plasma experiment as compared to the nitrogen–hydrogen plasma. The peaks resulting from these two different experimental setups are displayed at 2920°C and 2475°C, respectively (Figs. 8 and 5). Both peaks deviate approximately 200°C from the melting temperature of ZrO_2 (2670°C), which corresponds to approximately 7–8% of the measured value. In both experiments, the same material was used and it is most likely that the deviation in absolute temperature is due to inherent inaccuracies [in the two color pyrometry technique] such as different calibration setups (DPV 2000 is calibrated against a pre-calibrated tungsten lamp), or deviation from grey body assumption (of the ZrO_2) during liquid–solid phase transformation. Therefore, the results here also suggest that the location of peak 'G1' can be linked to the melting temperature.

It is an interesting fact about these peaks that although produced with different plasma generators, measured with different equipment and displayed at different absolute temperatures, the distribution structures seem to provide information about the melting status of the particles.

3.1.6. Arc Root Fluctuation Effects

Experimental results and theoretical calculations(44–46) suggest that arc root fluctuations could lead to segregation effects producing waves of 'cold' and 'hot' particles. Arc root fluctuations cause the particles to experience fluctuations in the plasma field during their exposure time (travel through plume), resulting in clusters/bursts of particles being exposed to

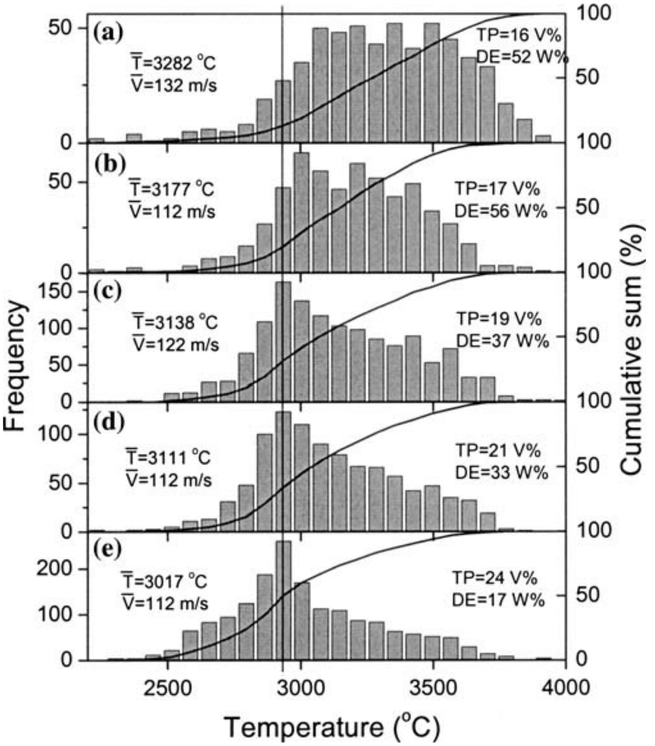

Fig. 8. Particle temperature distributions of increasing (from bottom to top) average temperatures for Ar-H_2 plasma.

an average higher or lower heat energy transfer. In order to detect this phenomenon, diagnostic measurements need to be carried out with a time resolved data acquisition such that accuracy of time measurement is higher than the expected arc root fluctuation frequency. In our current diagnostic instruments, this could not be achieved and hence there is no information about time-dependent phenomena in this data set that could be used to confirm or deny the effect of arc root fluctuations on the temperature distributions. However, for the present standoff distance (130 mm) and a nominal particle velocity of 100 m/s, the particle residence time is of the order of 1.3 ms. Using a predominant arc root fluctuation frequency of 6 kHz, the number of fluctuations a particle typically experiences would be of the order of 8, and the effect is likely to be averaged out. In addition, a companion paper (titled "A Critical Assessment of Particle Temperature Distributions During Plasma Spraying: Numerical Studies for YSZ") to this paper in the same journal has also observed the presence of such structures in particle temperature distributions generated using computation. Arc root fluctuations have not been considered in their model and the fact that these structures are reproduced in absence of this assumption reinforces the hypothesis that these are not the cause of origin of the peaks.

3.1.7. Analysis of Peaks 'G2' and 'G3'

As seen in Fig. 2, the overall temperature distribution can be mathematically described by three underlying gauss curves. Evidence has been presented to show that the peak 'G1' originates from solid–liquid phase change at the melting temperature due to the associated latent heat.

In this section, we take a closer look at the origin of peaks 'G2' and 'G3' with respect to size segregation. Figure 9 shows the histograms O, H and A (selected over a significant change in average temperature) from Fig. 4 to examine differences. In Fig. 9, within each histogram, temperature zones close to the peaks 'G1', 'G2' and 'G3' are highlighted. Figure 10, depicts the particle distributions that are associated with each of these highlighted temperature zones. In each chart within Fig. 10, a smooth curve is overlaid on the histograms. This curve is the distribution function of all the particles detected during the measurement and allows comparison of the overall distribution with the individual ones corresponding to each of the peaks – 'G1', 'G2' and 'G3'. The number displayed in Fig. 10 denotes the number of particles in that histogram.

Considering the low temperature condition represented by 'A', the peak 'G1' displays an average temperature of 2496°C which is fairly close to the peak temperature of 2475°C. This peak also has a particle size distribution that is representative of the overall size distribution. This implies that a representative part of the overall particle population is at the melting point. At the slightly higher temperature condition 'H', it can be seen that the particles contributing to 'G1' are no longer representative of the overall population. Only the larger size fraction is now at the melting point. In this case, the 'G2' peak now has size distribution representative of the overall particle population. At the highest temperature as represented by histogram 'O', the 'G3' peak has particles that show a size distribution similar to the overall particle distribution. Essentially, at higher temperatures, the peaks 'G2' and 'G3' become more prominent, but unlike the 'G1' peak temperature, the location of these two is not fixed. The peaks 'G2' and 'G3' are controlled by the net power, temperature distribution within the plasma, the original size distribution and their interaction. As of now, out data does not allow for a precise physical interpretation

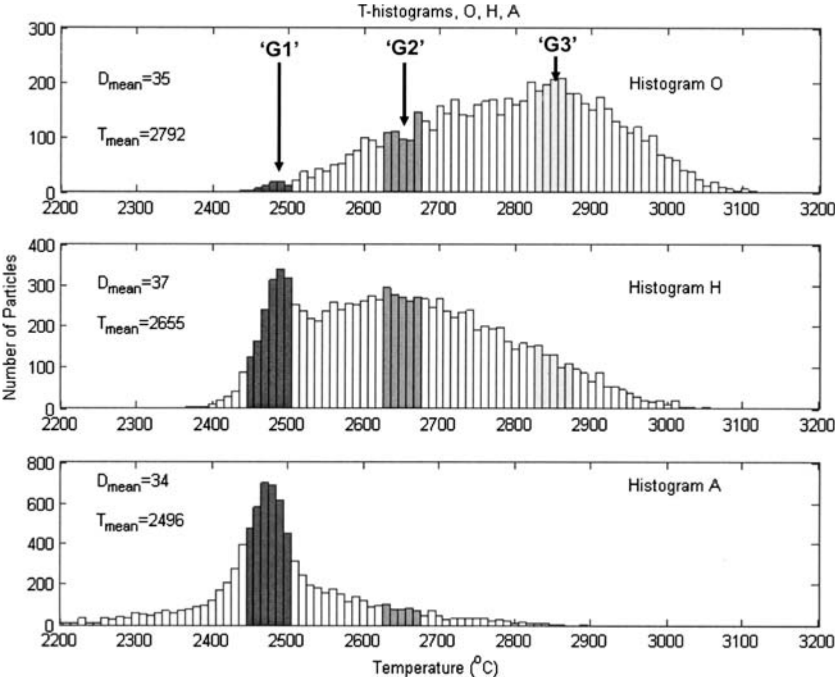

Fig. 9. Temperature distributions for three of the conditions 'A', 'H' and 'O' as shown in Fig. 4 with the different peaks 'G1', 'G2' and 'G3' selected to examine the corresponding size distributions within each.

of these peaks, but a statistical analysis of these has been presented to explain the occurrence.

The following hypothesis is presented as a possibility. This will need more evidence in order to be confirmed. A possible explanation can be the transparency effects leading to the 'G2' and 'G3' peaks. Consider that the spray stream contains two kinds of particle species – the one set that are transparent/semi-transparent and the others that are opaque. In case of the opaque particles, radiation is emitted only from the surface. Transparent particles however radiate from the surface and from inside the bulk, so the two color temperature as estimated by the pyrometer could be between 200 and 300 degrees higher or lower than on the surface and would depend on the temperature gradients within the particles.$^{(42)}$ When the temperature gradient is small, opaque and transparent particles would show nearly the same temperature and 'G2' and 'G3' would be close together. When the temperature gradient is large 'G2' and 'G3'

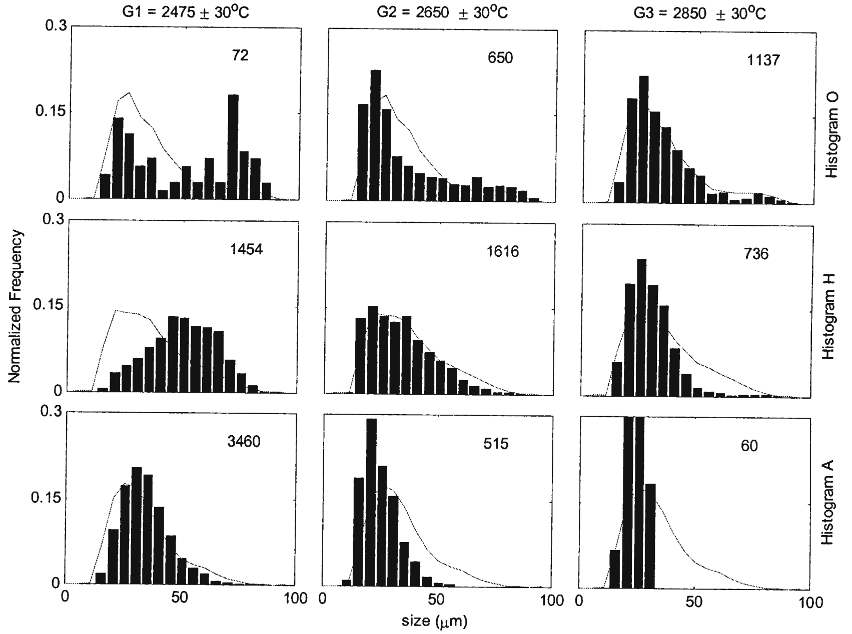

Fig. 10. Particle size distributions at the peaks 'G1', 'G2' and 'G3' for the conditions 'A', 'H' and 'O' from within different parts of the temperature distributions (as depicted in Fig. 9).

will be further apart. To some extent this effect is seen in Fig. 11. As the H_2 content in the plasma is increased, the thermal conductivity of the gas increases and leads to lower gradients. This has the effect of bringing the two peaks closer.

3.2. Implications of Distribution Variations

The previous sections have demonstrated that to a first approximation, the shape of temperature distributions is controlled by the mean temperature. While this is true when examining the large range of process conditions as shown in Fig. 4, by itself, this rule is not a sufficient guideline in the central area of the process window (e.g. condition 'H' in Fig. 4). The overview of temperature regimes in Table II shows the combinations possible to achieve a state. As can be seen, at the process window extremes, the number of combinations that can result in a given particle state are minimum or even unique (limited by the operational range of the hardware). At other locations inside the 'process window', any given point (defined by the average velocity and temperature) can

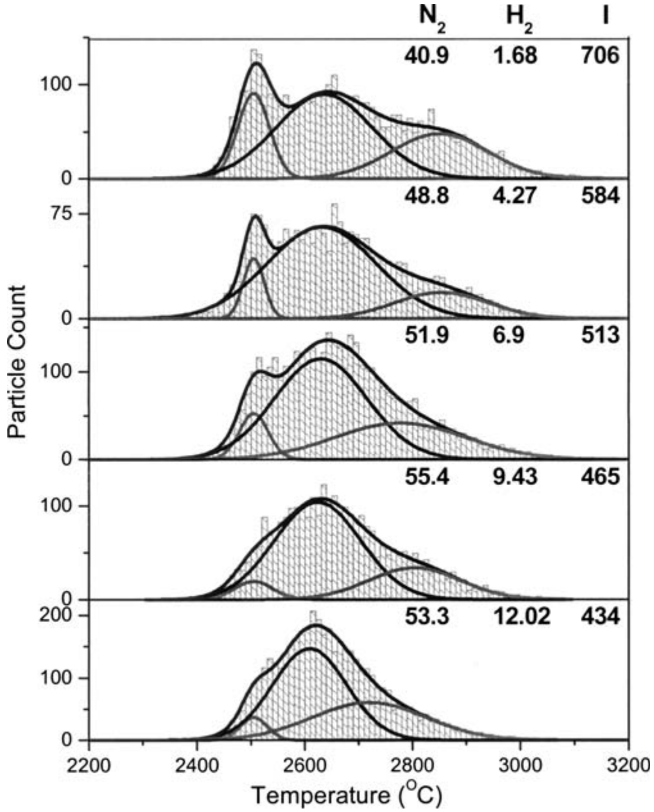

Fig. 11. Variation in temperature distributions where the average temperature and velocity are the same (average values within ±5°C and ±2.5 m/s, respectively). The underlying distributions are dependent on the specific combination of operating parameters chosen (these are listed for each distribution in the order N_2 flow, H_2 flow and gun current). The distributions have been arranged in the sequence of increasing H_2 flow (from top to bottom) and each has been fitted with a combination of three Gauss peaks.

be attained by a wide variety of combinations of the primary gun control parameters. These intermediate temperature and velocity states more or less define a transition regime in which particle melting state is most sensitive to a change in gun parameters. Much of this variability is a result of the similar effects that the secondary gas flow and amperage have on the average particle temperature. An experimental verification of this hypothesis is possible since it has been shown(17,18,35) that temperature and velocity can be controlled independently. Using the results of our '1st order process map', we were able to use an iterative procedure (typically

Table II. A Control Regime in Which Temperature Distributions can Vary Significantly Although Average T and V are Held Constant

Temperature range	Possible melting state variations	Possible primary gun parameter combinations
High	None: all particles molten	One: all parameters to maximum
Medium	Melting transition	Many combinations; 'Same T and V problem'
Low	Large fraction of particles unmolten	One: all parameters to minimum

between one and seven iterations) to lock into a predefined mean temperature/velocity state (T = 2661°C, V = 125 m/s). The procedure was based on DPV 2000 single point measurements in the flow center and on achieving constant mean particle trajectory. By pre-setting either the secondary flow or the amperage it is possible to achieve the same temperature and velocity state with largely different primary gun parameter settings (Table III).

The robustness of this empirical non-linear model (resulting from the experimental data) is evident from the fact that pre-setting any one of the complementary values of the control parameters and optimizing the other two results in the same set of triplet of primary parameters. For e.g., if the secondary gas flow was to be fixed at 1.7 slpm and the model used to generate values of primary flow and gun current (to attain a mean temperature and velocity of 2661°C and 125 m/s), the values obtained would be 40.9 slpm and 706 A. On the other hand if the Gun current was fixed at 706 A, the values of primary and secondary gas flows would come out to be 40.9 and 1.7 slpm.

Figure 11 exhibits the change in temperature distributions when the torch conditions are set according to Table III (primary, secondary gas flow and gun current). In all these cases, the average temperature and velocity was controlled with an accuracy better than $\Delta T = 10°C$ and

Table III. Plasma Torch Control Parameter Settings Used to Achieve a Mean Temperature/Velocity State of $T = 2661 \pm 5°C$ and $V = 125 \pm 2.5$ m/s. Input Power has been Calculated Assuming an Efficiency of 0.7 (as in the Modeling) of the Total Power

Primary gas (N_2, Slpm)	Secondary gas (H_2, Slpm)	Gun Current (A)	Voltage (V)	Input power (total power, kW)
40.9	1.7	706	68.5	33.8 (48.4)
48.8	4.3	584	73.7	30.1 (43.0)
51.9	6.9	513	79.3	28.5 (40.7)
55.4	9.4	465	82.2	26.8 (38.2)
53.3	12	434	83.5	25.4 (36.2)

$\Delta V = 5\,\mathrm{m/s}$ (specifically, this data is for the hollow spherical morphology of the YSZ feed stock).

With increasing H_2 level from top to bottom, the distributions become narrower, since the high temperature 'tail' is shifted to lower temperatures and at the same time the significant melting indicator peak 'G1' loses intensity while staying at a constant temperature of 2475°C. To quantify this systematic transition, a gauss fitting approach was used with the three separate peaks. The overall shape of the distributions can be captured quite accurately ($R^2 > 0.99$).

A possible explanation for the observed, systematic changes can be the improved heat transfer at higher H_2 levels. Although the electrical input power and thus the enthalpy of the plasma is lower, the enhanced heat transfer results in a more uniform heating of the particles which narrows the temperature distributions (while displaying the same average T and V). Increased hydrogen content in the plasma flame influences the particle temperatures but has almost no effect on the velocity. The regression fit to obtain particle velocity and temperature as a function of hydrogen content, mass flow and torch current clearly demonstrate this. Particle speed is governed by the total mass flow of the gases and the nozzle geometry.

3.2.1. Variation in Coating Properties

For each of the conditions described in the section above, deposits were also made. The characteristic properties of these deposits are being examined in detail to understand the variations that result in structure of the coating as a consequence of these changes in temperature distributions. Figures 12 and 13 are presented as an overview of the differences in the coating properties and structures. It is observed that increasing the hydrogen flow values (but keeping the same average particle temperature and velocity) leads to an increase in the deposition efficiency. There is also a decrease in the coating porosity when going from low hydrogen flow to high flow. It is envisioned that this part of the study would provide very important guidelines to the control aspect of plasma spray parameters.

4. CONCLUSIONS

A systematic examination of temperature distributions of particle at the deposition location during plasma spraying of YSZ has been presented. A 3D integrated diagnostic set-up along with point to point measurement of particle parameters has been developed. A tri-modal structure has been observed in the temperature distribution from which a significant

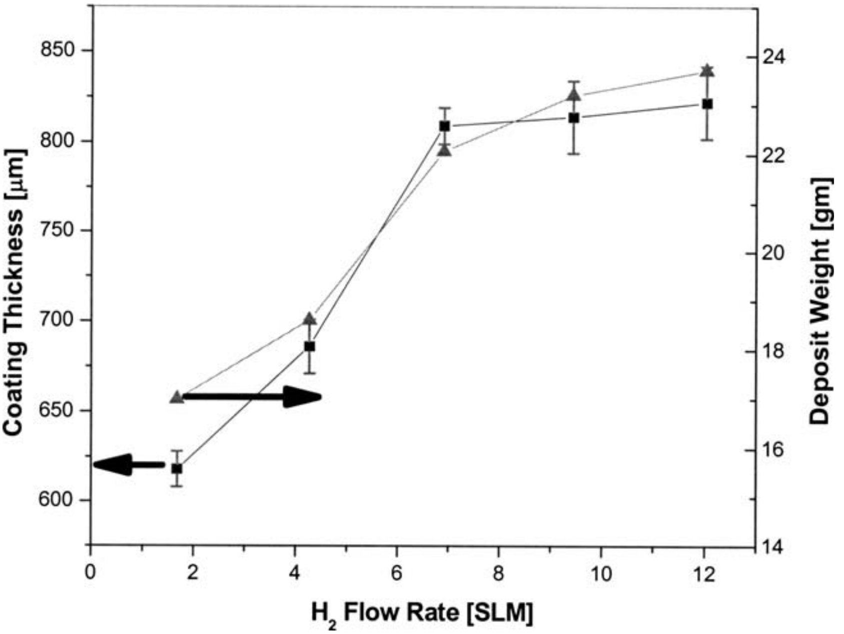

Fig. 12. The change in deposit properties as a function of the hydrogen percentage (while maintaining equal average temperature and velocity of the particles). As can be seen, the relative deposit efficiency as indicated by the coating thickness and weight changes significantly with the hydrogen flow level values (corresponding to the temperature distributions shown in Fig. 11).

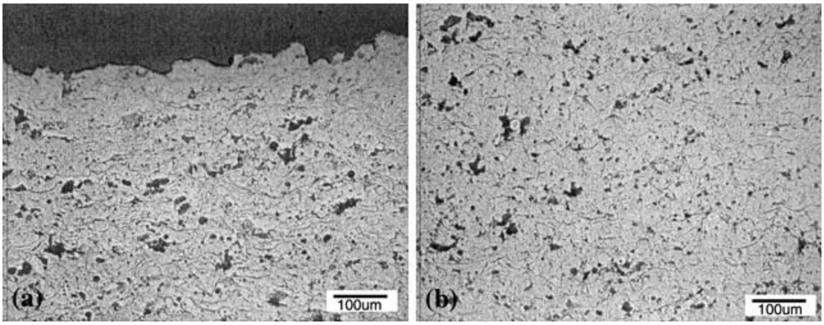

Fig. 13. Microstructures of coatings deposited with the same average particle velocity and temperature but (a) low hydrogen flow (1.68 slm) and (b) high hydrogen (12.02 slm) flow plasma conditions as shown in Fig. 11. The high hydrogen condition shows slightly lower porosity.

melting peak can be extracted. This melting peak is at a constant temperature (for a given calibration setting of the pyrometric detector) and is independent of particle size, powder morphology and process parameters. The second and third peak correspond to the particle temperature distributions that relate to process conditions and can therefore be ruled out as a melting state indicator.

It has further been shown through these results that hollow spherical powders are indeed easier to melt compared to powders of solid morphologies. Process parameters do influence the extent of melting of particles and their effect can be better understood by analysis of the histograms of the particle temperature distributions.

It has further been shown that one can achieve significantly different particle temperature distributions for a given average value. Although this is not surprising, the extent to which the distributions can be manipulated is an important finding. In general the shape of the temperature distributions changes with average temperature. In the central region of the maximum process window, this approach is insufficient and it is necessary to look at the distributions themselves to draw conclusions on the melting state. This suggests that the traditional approach to process control based on average particle temperatures and velocities needs to be carefully considered. For monitoring in this parameter space, the plume width might be a good control parameter.

These experimental findings have also been compared with 3D numerical modeling of the plasma spray process. These results have important implications particularly for YSZ coatings where deposit efficiency and microstructure are critical attributes of their processing, performance and reliability. Follow-on studies linking these particle state findings to the deposit characteristics are underway.

ACKNOWLEDGMENTS

This research was sponsored by the MRSEC program of the National Science Foundation under award DMR 0080021. Partial support obtained through the consortium on thermal spray technology at Stony Brook is acknowledged. Authors gratefully acknowledge the comments of Dr. C. Moreau and Dr. R. Neiser on the present findings.

REFERENCES

1. C. Moreau, M. Lamontagne, and P. Cielo, Method and apparatus for monitoring the temperature and velocity of plasma sprayed particles, US Patent 5,180,921.

2. C. Moreau, P. Gougeon, M. Lamontagne, V. Lacasse, G. Vaudreuil, and P. Cielo, On-line control of the plasma spraying process by monitoring the temperature, velocity and trajectory of in-flight particles, in *7th National Thermal Spray Conference*, (S. Sampath and C. C. Berndt, eds.), ASM International, Boston, Massachusetts, 1994, pp. 431–438.
3. M. L. Yeoman, B. J. Azzopardi, H. J. White, C. J. Bates, and P. J. Roberts, Optical development and application of a two colour LDA system for the simultaneous measurement of particle size and particle velocity, in *Engineering Applications of Laser Velocimetry*, American Society of Mechanical Engineers, Phoenix, AZ, 1982, pp. 127–135.
4. T. Streibl, K, D. Landes, and G. Forster, PSI: New diagnostics for the determination of particle size and shape in thermal spray processes, in *1st International Thermal Spray Conference*, (C. C. Berndt, ed.), ASM International, Motreal, Quebec, Canada, 2000, p. 67.
5. S. Zimmermann and K. Landes, *Microstruct. Process.* **383**, 153 (2004).
6. J. R. Fincke, D. C. Haggard, and W. D. Swank, *J. Thermal Spray Technol.* **10**, 255 (2001).
7. J. R. Fincke, W. D. Swank, R. L. Bewley, D. C. Haggard, M. Gevelber, and D. Wroblewski, *Surf. Coat. Technol.* **146**, 537 (2001).
8. W. D. Swank, J. R. Fincke, and D. C. Haggard, A Particle temperature sensor for monitoring and control of the thermal spray process, in *Thermal Spray Science and Technology: Proceedings of the 8th National Thermal Spray Conference*, ASM International, Houston, Texas, US, 1995.
9. J. Vattulainen, E. Hamalainen, R. Hemberg, P. Vuoristo, and T. Mantyla, *J. Thermal Spray Technol.* **10**, 94 (2001).
10. J. F. Bisson, M. Lamontagne, C. Moreau, L. Pouliot, J. Blain, and F. Nadeau, Ensemble in-flight particle diagnostics under thermal spray conditions, in *Thermal Spray 2001: New Surfaces for a New Millennium*, ASM International, Singapore, 2001.
11. G. Bourque, M. Lamontagne, and C. Moreau, A new sensor for on-line monitoring the temperature and velocity of thermal spray particles, in *1st International Thernnal Spray Conference*, (C. C. Berndt, ed.), ASM International, Montreal, Quebec, Canada, 2000, p. 45.
12. J. Zierhut and K. D. Landes, Particle flux imaging (PFI) in-situ diagnostics for thermal coating processes, in *1st International Thermal Spray Conference*, (C. C. Berndt, ed.), ASM International, Montreal, Quebec, Canada, 2000, p. 63.
13. H. Zhang, H. B. Xiong, L. L. Zheng, A. Vaidya, L. Li, and S. Sampath, Melting behavior of in-flight particles and its effects on splat morphology in plasma spraying, in *International Mechanical Engineering Congress and Exposition*, ASME International, New Orleans, Louisiana, USA, 2002, pp. 1–8.
14. G. Wei, H. Xiong, L. Zheng, and H. Zhang, Modeling from particle in-flight to coating build-up for thermal spray processes, in *ASME Heat Transfer/Fluids Engineering Summer Conference*, ASME, Charlotte, North Carolina, USA, 2004.
15. P. Fauchais, M. Vardelle, A. Vardelle, L. Bianchi, and A. C. Leger, *Plasma Chem. Plasma Process.* **16**, S99 (1996).
16. P. Fauchais, M. Vardelle, A. Vardelle, and L. Bianchi, *Ceram. Int.* **22**, 295 (1996).
17. M. Friis, C. Persson, and J. Wigren, *Sur. Coat. Technol.* **141**, 115 (2001).
18. M. Prystay, P. Gougeon, and C. Moreau, *J. Thermal Spray Technol.* **10**, 67 (2001).
19. R. Mcpherson, *Surf. Coat. Technol.* **39/40**, 173 (1989).
20. P. Bengtsson, T. Johannesson, and J. Wigren, *J. Thermal Spray Technol.* **4**(3), 245 (1995).

21. M. Vardelle, A. Vardelle, P. Fauchais, and C. Moreau, *Meas. Sci. Technol.* **5**, 205 (1994).
22. M. Vardelle, A. Vardelle, A. C. Leger, P. Fauchais, and D. Gobin, *J. Thermal Spray Technol.* **4**, 50 (1995).
23. D. Gilmore, R. Neiser, Y. Wan, and S. Sampath, Process maps for plasma spray Part I: Plasma–particle interactions, in *Thermal Spray Surface Engineering via Applied Research (Proceedings of the 1st ITSC, May 2000)*, (C. C. Berndt, ed.), ASM International, Materials Park, 2000, pp. 149–155.
24. X. Jiang, J. Matejicek, A. Kulkarni, H. Herman, S. Sampath, D. Gilmore, and R. Neiser, Process maps for plasma spray Part II: Deposition and properties, in *Thermal Spray Surface Engineering via Applied Research (Proceedings of the 1st ITSC, May 2000)*, (C. C. Berndt, ed.), ASM International, Materials Park, 2000, pp. 157–163.
25. S. Sampath, X. Jiang, A. Kulkarni, J. Matejicek, D. L. Gilmore, and R. A. Neiser, *Mater. Sci. Eng. A* **348**, 54 (2003).
26. S. Sampath, X. Y. Jiang, J. Matejicek, L. Prchlik, A. Kulkarni, and A. Vaidya, *Mater. Sci. Eng. A* **364**, 216 (2004).
27. A. Vaidya, T. Streibl, L. Li, S. Sampath, A. Gouldstone, O. Kovarik, and R. Greenlaw, Comprehensive study of the process–property correlations: Case study for molybdenum coatings, in *ITSC 2004, Thermal Spray Solutions: Advances in Technology and Application*, Electronic Publication, Osaka, Japan, 2004.
28. M. Vardelle, A. Vardelle, A. C. Leger, and P. Fauchais, Dynamics of splat formation and solidification in thermal spraying process, in *Thermal Spray Industrial Applications*, (C. C. Berndt and S. Sampath, eds.), ASM International, Materials Park, OH, USA, Boston, MA, 1994, pp. 555–562.
29. S. Fantassi, M. Vardelle, A. Vardelle, and P. Fauchais, *J. Thermal Spray Technol.* **2**, 379 (1993).
30. L. Bianchi, F. Blein, P. Lucchese, M. Vardelle, A. Vardelle, and P. Fauchais, Effect of particle velocity and substrate temperature on alumina and zirconia splat formation, in *Thermal Spray Industrial Applications*, (C. C. Berndt and S. Sampath, eds.), ASM International, Materials Park, OH, USA, Boston, MA, 1994, pp. 569–574.
31. J. Madejski, *Int. J. Heat Mass Transfer*. **19**, 1009 (1976).
32. Y. P. Wan, H. Zhang, X. Y. Jiang, S. Sampath, and V. Prasad, *J. Heat Transfer-Trans.* ASME **123**, 382 (2001).
33. H. Zhang, *Int. J. Heat Mass Transfer*. **42**, 2499 (1999).
34. A. Vaidya, G. Bancke, S. Sampath, and H. Herman, Influence of process variables on the plasma sprayed coatings: An integrated study, in *International Thermal Spray Conference (ITSC)*, (B. C. C. and K. K. A., eds.), ASM International, Materials Park, OH, Singapore, 2001, pp. 1345–1349.
35. M. Friis, P. Nylen, C. Persson, and J. Wigren, *J. Themal Spray Technol.* **10**, 301 (2001).
36. M. Friis, and P. Nylén, A numerical study of the sources of variation in particle in-flight characteristics in atmospheric plasma spraying, in *Thermal Spray 2003: Recognizing the Past, Supporting the Future and Nurturing Prosperity*, (C. C. Berndt, ed.), ASM International, Materials Park, OH, USA, Orlando, FL, 2003.
37. S. Guessasma, G. Montavon, and C. Coddet, *Surf. Coat. Technol.* **192**, 70 (2005).
38. D. Scott, *Biometrika* **66**, 605 (1979).
39. D. Ng, Two-step calibration of a multiwavelength pyrometer for high temperature measurement using a quartz lamp, NASA/TM-2001-211124, Glenn Research Center, Cleveland, Ohio, 2001.
40. D. Ng and G. Fralick, *Rev. Sci. Instrum.* **72**, 1522 (2001).

41. V. A. Petrov and A. P. Chernyshev, *High Temp*. **37**, 58 (1999).
42. L. A. Dombrovsky, *J. Quant. Spectrosc. Radiative Transfer*. **73**, 433 (2002).
43. M. Friis and C. Persson, *J. Thermal Spray Technol*. **12**, 44 (2003).
44. J. F. Bisson and C. Moreau, *J. Thermal Spray Technol*. **12**, 258 (2003).
45. J. F. Bisson, B. Gauthier, and C. Moreau, *J. Thermal Spray Technol*. **12**, 38 (2003).
46. P. Fauchais, *J. Phys. D: Appl. Phys*. **37**, 86 (2004).